PROCEEDINGS, 49th Workshop on Geothermal Reservoir Engineering
Stanford University, Stanford, California, February 12-14, 2024
SGP-TR-227

The effect of temperature on the static elastic moduli of fractured granitoid from the Patua geothermal field

Harrison P. Lisabeth[1*], Nori Nakata[1], Heather M. Savage[2] and Kristina K. Okamoto[2]

[1]Lawrence Berkeley National Laboratory, 1 Cyclotron Rd., Berkeley, CA 94720

[2]University of California, Santa Cruz, 1156 High St., Santa Cruz, CA 95064

[*]hlisabeth@lbl.gov

Keywords: geomechanics, fractured rocks, thermo-mechanical, microstructure

ABSTRACT

Adaptive control of geothermal systems requires high-fidelity knowledge of the mechanical behavior of reservoir rock and the response of materials to thermal and mechanical stresses. The presence of large fractures and smaller microcracks in otherwise low porosity igneous rocks makes the mechanical behavior highly stress- and temperature-dependent. We present the results of a suite of laboratory measurements of the static elastic properties of a fractured granitoid rock from the Patua geothermal field. Measurements were made from 10-70 MPa confining pressure and from room temperature to 150°C. We find that both increases in confining pressure and increases in temperature up to 150°C increase elastic moduli and stress-dependent behavior is observed within the entire range of experimental conditions. We interpret this behavior to be the result of the interaction between large and small fractures within the rock. These results are discussed within the context of reservoir geomechanics and the response of geothermal systems to thermal, hydraulic and mechanical perturbation.

1. INTRODUCTION

Geothermal energy generation promises to be an integral component of a clean energy system due to its ability to contribute base load power in complement to the intermittent power produced by wind and solar energy (Azim et al., 2010). By some estimates, geothermal plants have the potential to produce 100 GW of power by 2050 in the United States (Tester et al., 2006); however, this estimate hinges on the development of enhanced geothermal systems (EGS) in this timeframe. Successful operation of EGS requires advanced control of reservoir geomechanical and hydraulic behavior (Ghassemi, 2012; White et al., 2018) as well as mitigation of seismicity (Majer et al., 2007). Each of these challenges demands operational knowledge of the thermo-hydro-chemo-mechanical (THMC) properties of the reservoir materials.

This paper presents the results of a suite of mechanical tests on a granodiorite specimen from the Patua geothermal field. This sample is typical of many EGS reservoirs; it is a fractured, coarse-grained, plutonic igneous rock. We conduct a series of cyclical loading tests, both hydrostatic and deviatoric, at a range of confining pressures (10-70 MPa) and temperatures (23-150°C) and use the recorded stress and strain behavior to estimate the static bulk and shear moduli of our sample. We perform microstructural and chemical analysis of our materials and discuss the temperature and pressure dependencies of the elastic properties in context of fracture structure and mineralogy.

2. EXPERIMENTAL DETAILS

2.1 Sample material

Sample material was received as a 3-inch core in a polyolefin jacket. This core material was recovered from a cataloged core repository without adequate labeling, but the appearance, structure and mineralogy of the core suggest it is from the primary reservoir from a depth greater than ~4500 ft (Cladouhos et al., 2017). The larger core was sub-cored into a 1.50-inch diameter by 2.41-inch long sample with ends ground parallel to 0.001 inches (Figure 1a). Remaining scrap material was used to prepare a 30-micron thin section slide for petrography scanning electron microscope (SEM) and energy dispersive spectroscopy (EDS) analysis. The sample was oven dried at 50°C overnight and weighed for a dry mass of 179.98g. The final sample had a single fracture apparent on the side of the core at approximately 75° to the core axis. We estimate the aperture to be close to 250 microns where it intersects the edge of the sample. The sample remained intact, so the fracture was not through going. Petrographic estimates of sample mineralogy are 70% feldspar, 28% quartz and 2% biotite/chlorite with trace iron oxides and apatite. The sample displayed no clear oriented fabric and exhibited significant grain boundary microcracks.

2.1 Experimental Procedure

The sample was mounted on endcaps and jacketed with viton to separate the rock material from the confining medium. Two linear and one radial linear variable differential transformers (LVDT) were affixed to the sample assembly (Figure 1b). Aluminum stubs were epoxied into the jacket to ensure radial LVDT contact with the specimen.

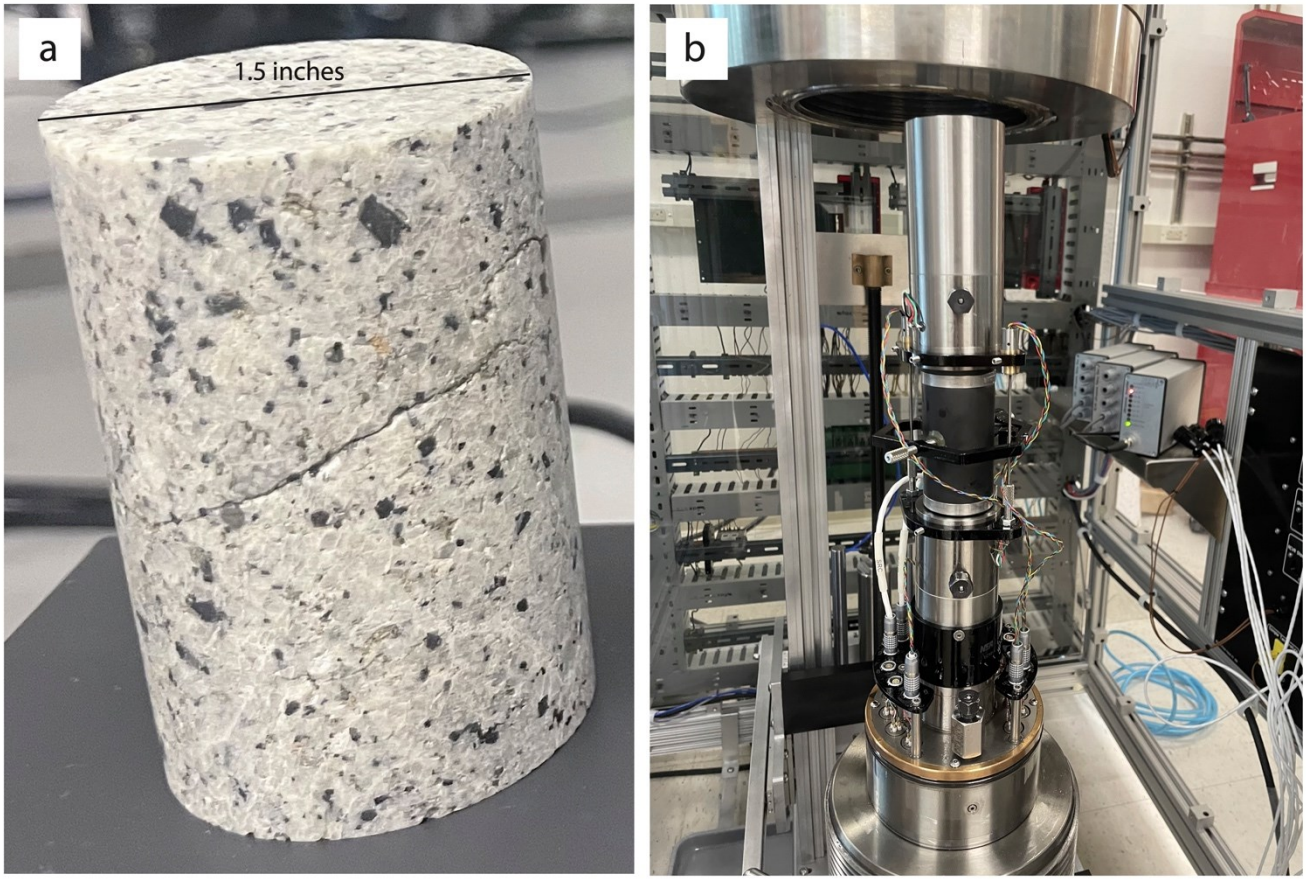

Figure 1: Photographs of a) core sample and b) jacketed and instrumented sample.

Initial measurements were made at room temperature, 23°C. Once loaded into the pressure vessel, the sample was first seated by pressurizing and depressurizing the system to the ultimate pressure several times. The confining pressure was then raised to 10 MPa and a small end load of 1.5 MPa applied to the sample. The confining pressure was then cycled by 5 MPa three times at a loading rate of 2 MPa/minute. The axial load was then cycled 5 MPa three times at a loading rate of 2 MPa/minute, while the confining pressure was reduced to maintain a constant mean stress. The confining pressure was then increased by 10 MPa and this procedure repeated. Pressure steps increased by 10 MPa up to 70 MPa, then were reduced by 20 MPa at a time until the initial confining pressure of 10 MPa was reached (Figure 2). The temperature of the system was then increased to 90°C and allowed to thermally equilibrate for 10 hours. The loading procedure was repeated then the temperature raised a final time to 150°C and allowed to thermally equilibrate for another 10 hours. After a final loading procedure, the sample was cooled and removed from pressure vessel. The triaxial rig can achieve confining pressures of 400 MPa, a maximum axial force: 2.6 MN, and temperatures to 300°C. The internal load cell and the confining pressure transducer have an accuracy of 0.5%. The internal vertical LVDTs have a 6-mm range and a resolution of ~0.1µm.

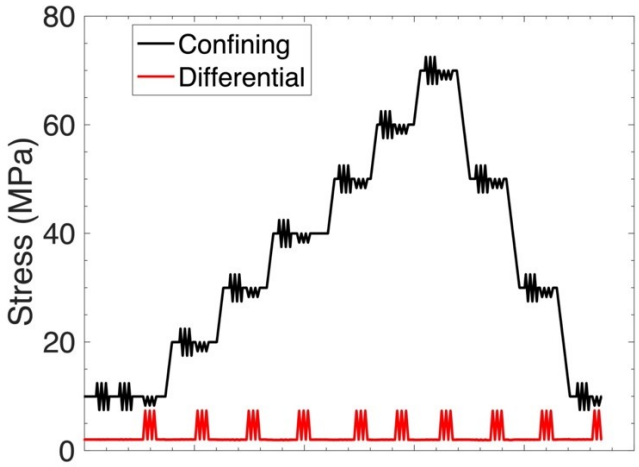

Figure 2: Loading path for experiments.

3. RESULTS

3.1 Estimation of static elastic parameters

Sample strain was calculated from axial and transverse displacements as measured by LVDTs.

$$\varepsilon_a = \frac{d_a}{L} \tag{1}$$

$$\varepsilon_t = \frac{d_t}{D} \tag{2}$$

Where ε_a, ε_t, d_a, d_r, L, and D are axial strain, transverse strain, axial displacement, transverse displacement, sample length and sample diameter, respectively. Axial displacement is taken to be the average of the two axial LVDTs. For an axisymmetric sample, volumetric and distortional strain are calculated,

$$\varepsilon_v = \varepsilon_a + 2\varepsilon_t \tag{3}$$

$$\varepsilon_s = \frac{2}{3}(\varepsilon_a + 2\varepsilon_t) \tag{4}$$

Where ε_v and ε_s are volumetric and distortional strain respectively. We then define mean stress and differential stress as,

$$p = \frac{1}{3}(\sigma_a + 2\sigma_t) \tag{5}$$

$$q = \sigma_a - \sigma_t \tag{6}$$

Where p, q, σ_a and σ_t are mean stress, differential stress, axial stress and transverse stress, respectively. Transverse stress is taken to be the confining pressure and axial stress is the sum of the load cell stress and confining pressure. We can then calculate the bulk and shear moduli for an axisymmetric sample as,

$$K = \left.\frac{\partial p}{\partial \varepsilon_v}\right|_q \tag{7}$$

$$G = \left.\frac{\partial q}{\partial \varepsilon_s}\right|_p \tag{8}$$

Where K and G are the bulk and shear modulus. Slopes of the stress strain curves are evaluated during each cyclic loading cycle. Stress strain curves for the full experiment are presented in Figure 3.

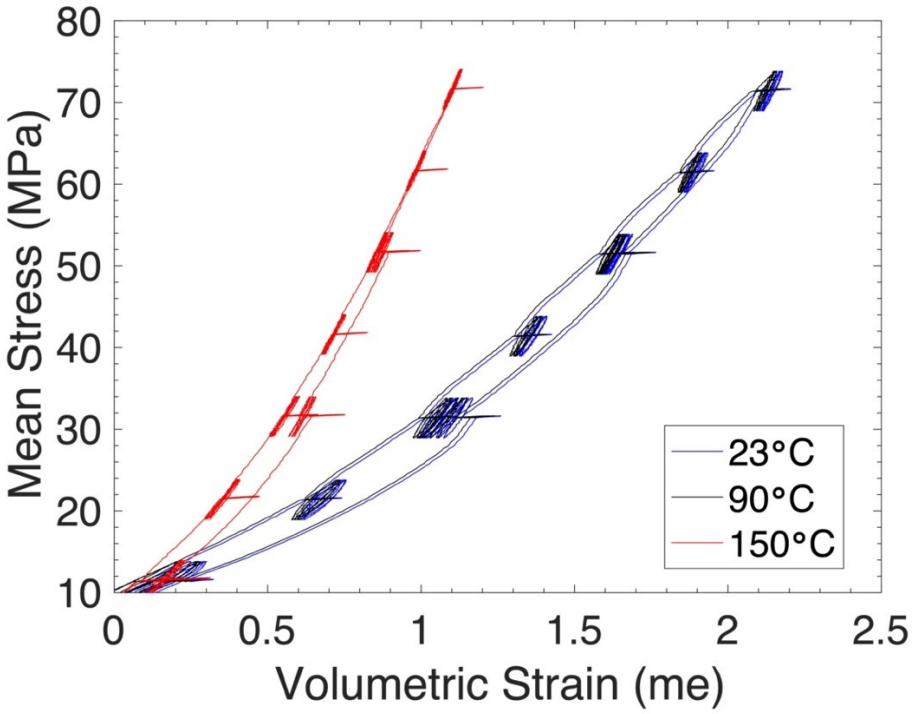

Figure 3: Stress-strain data from full experiments at all temperatures.

3.2 Hydrostatic compression

Bulk modulus shows a positive correlation with confining pressure at all temperatures (Figure 4a). At room temperature, the bulk modulus of the sample increases from 19.6 to 54.5 GPa over the range of confining pressures from 10 to 70 MPa. The sample shows little hysteresis in modulus upon unloading. At 90°C, the bulk modulus increases from 19.2 to 65.1 GPa across the pressure range, again exhibiting little hysteresis. At 150°C, the bulk modulus exhibits significantly higher bulk modulus at elevated pressure, increasing from 23.2 to 84.1 GPa. At the highest temperature, the bulk modulus did exhibit some hysteresis upon unloading, suggesting some irreversible change may have occurred. After unloading to 10 MPa confining pressure at 150°C, the final bulk modulus was 34.9 GPa, a 50% increase from the initial modulus.

At all temperatures, the modulus-pressure curves are concave downwards, demonstrating progressively smaller increments of bulk modulus increase as pressure is raised. This behavior is consistent with the progressive closure of microcracks (Walsh, 1965) and/or the stiffening of larger fractures due to the growth of asperities (Hopkins et al., 1987; Lisabeth and Ajo-Franklin, 2023). At 10 and 20 MPa confining pressure, the room temperature and 90°C data are very similar, but as the pressure increases the behavior begins to deviate and the elevated temperature sample exhibits a higher bulk modulus. The sample at 150°C has both higher bulk modulus and a greater increase in modulus with pressure. If a line is fit the quasi-linear portion of the overall mean stress volumetric strain curve, overall bulk moduli of 35.6, 36.3 and 76.0 GPa are recovered for the room temperature, 90°C and 150°C experiments, respectively.

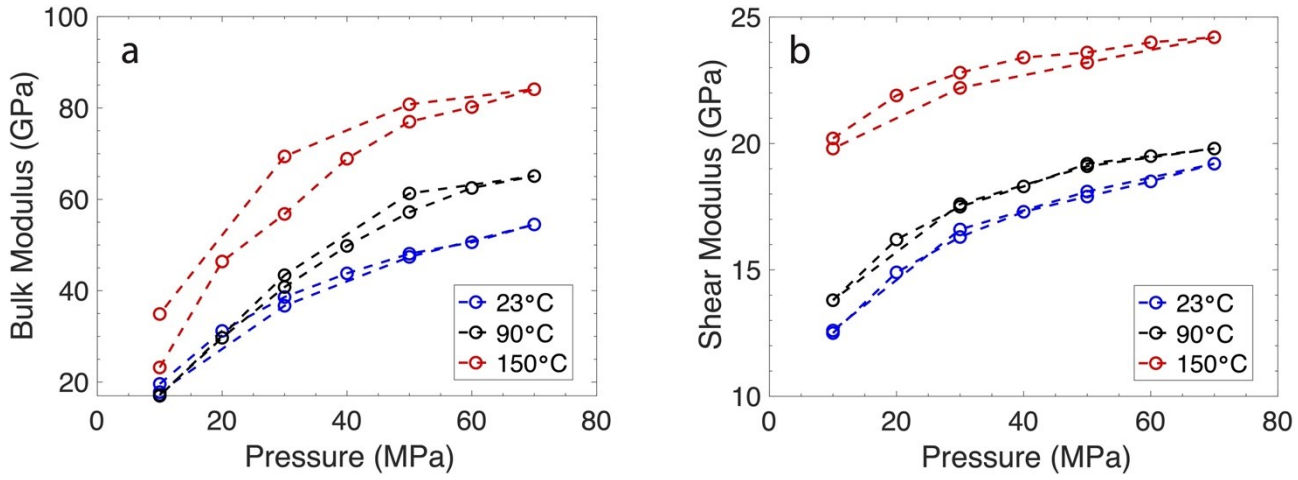

Figure 4: Static moduli for all experiments. a) Bulk modulus and b) shear modulus versus confining pressure.

3.3 Deviatoric loading

Similar to the bulk modulus, the shear modulus shows a positive correlation with confining pressure at all temperatures (Figure 4b). At room temperature, the shear modulus of the sample increases from 12.5 to 19.2 GPa over the range of confining pressures from 10 to 70 MPa. The sample shows little hysteresis in modulus upon unloading. At 90°C, the shear modulus increases from 13.8 to 19.8 GPa across the pressure range, again exhibiting little hysteresis. At 150°C, the shear modulus again is significantly higher at all pressures, increasing from 20.2 to 24.2 GPa. The shear modulus also exhibits some hysteresis upon unloading, remaining lower than during loading in contrast to the bulk modulus. After unloading to 10 MPa confining pressure at 150°C, the final shear modulus was 19.8 GPa, only a 2% decrease from the initial modulus.

Again, at all temperatures, the modulus-pressure curves are concave downwards. This behavior suggests progressive closure of microcracks and/or larger fractures also reduces shear deformation, suggesting a modification of asperity geometry and contact area (Saltiel et al., 2017; Lisabeth and Ajo-Franklin, 2023). Samples at all temperatures exhibit similar pressure dependence and modulus-pressure curves appear parallel, but the overall modulus increases with temperature.

4. DISCUSSION

4.1 Comparison to literature

The general range of values measured in this study agrees with values published in the literature. Comparison and contrast highlight some important aspects of our data to consider. Westerly granite, a commonly used standard plutonic igneous rock, has an intact bulk modulus of 39 GPa and a shear modulus of 28 GPa at 30 MPa confining pressure. These values are reduced to 25 and 16 GPa, respectively, when samples are subjected to thermal cracking at 650°C (Blake and Faulkner, 2016). The intact value of bulk modulus is comparable to our value at 30 MPa confining pressure and room temperature, 38 GPa, while the thermally fractured value of shear modulus is closer to our measured value at the same conditions, 16 GPa. Another standard igneous rock, Sierra White granite, has a bulk modulus of 35 GPa at 30 MPa confining pressure and a shear modulus of 25 GPa (Martin III and Haupt, 1994), again comparable to our values with a slightly higher shear modulus. There is relatively less data on the static elastic properties of granodiorites in general. One study of a granodiorite from the Coso geothermal field showed its bulk modulus to be 27 GPa and shear modulus to be 35 GPa at 50 MPa confining pressure (Morrow and Lockner, 2006). These values are significantly different than those measured here. There is little information in the report regarding the sample mineralogy or structure, so it is difficult to assess the cause of this difference.

A more direct comparison can be made to previous measurements on the material from Patua. One previous study found the bulk modulus of the granodiorite reservoir material to be 38 GPa and the shear modulus to be 28 GPa at 30 MPa, confining pressure and room temperature (Kc et al., 2019). This bulk modulus is in good agreement with our data, but the shear modulus is higher than our value. This is likely the result of the large fracture in our sample. Fractures can have a larger effect on shear properties than on compressional properties at elevated pressure (Lisabeth and Ajo-Franklin, 2023). We can also compare our measured properties with those inferred from the field. Using sonic logs from the geothermal field, Smith et al. (2023) infer bulk moduli between 30 and 40 GPa and shear modulus between 18 and 30 GPa for the granodiorite. These numbers are also in the range consistent with our measurement, but some values from from Kc et al. (2019) were used to calibrate, so the ranges are not entirely independent.

4.2 The effect of temperature

At all pressures measured in this study, increases in temperature result in higher static elastic moduli. There are two possible contributions to this effect: (1) thermoelastic changes in the properties of the individual minerals and (2) changes in the porosity and pore structure of the sample. For the primary rock forming minerals in our sample, quartz, feldspar and biotite, elastic moduli are nearly

constant or only slightly vary with temperature between room temperature and 150°C. In single crystal measurements, quartz exhibits a maximum of 5% reduction in elasticity within this temperature range (Ohno, 1995). In aggregate samples, slight increases (<10%) between room temperature and 50°C followed by slight reductions back to room temperature values have been observed (Yang et al., 2017; Trnik et al., 2019). In indentation tests, similar nominal changes are observed for quartz, albite and biotite (Espinoza et al., 2023). We measure increases in bulk modulus up to 55% and increases in shear modulus up to 30% between room temperature and 150°C, so these thermoelastic changes alone cannot account for the full effect. This suggests that porosity and pore structure play a determining role.

Examining the microstructure of our sample can yield important insights into the mechanisms of the observed stiffening. A representative SEM image and chemical EDS maps are presented in Figure 5. The SEM image was captured with a Zeiss Evo microscope at 15 keV accelerating voltage with a backscattered electron detector, so the grayscale is proportional to the atomic mass of the specimen, with heavier elements appearing lighter. The EDS data was collected with an Oxford Instruments EDS detector. The sample has a complex, multiphase grain structure consisting primarily of quartz, feldspar, biotite, iron oxide and some trace phosphates. The oxide mineral has complex inclusions. The biotite has been damaged during the thin section polishing process and the internally damaged areas have been filled with epoxy, the dark color in the SEM image. The feldspar displays a perthitic texture with Na-rich blebs in a K-rich background. Each mineral contains some amount of internal porosity. This porosity tends to be very small (<2 microns), is roughly circular, and should have a limited effect on sample compliance (David and Zimmerman, 2011). The majority of the porosity exists along grain boundaries. This porosity is crack-like and can have a significant effect on the compliance and pressure sensitivity of the sample. Fractures like this can form via thermal cracking processes due to contrasting thermal expansion in the various minerals (Clark, 1966; Wang et al., 1989). These grain boundary cracks have been shows to result in significant reductions in elastic moduli and strength (Fredrich and Wong, 1986; Blake and Faulkner, 2016). These reductions are often recovered by the application of confining pressure. Wang et al. (1989) estimate the crack closure pressure for these types of cracks to be approximately 40 MPa, but this will vary rock to rock and maybe change if there is additional deformation.

The final type of porosity to consider is the large, through-going fracture imaged in Figure 1a. This mesoscale feature may be held open by asperities due to geometric mismatch between rough surfaces. This type of fracture can remain open at high confining pressures (Brace et al., 1968; Barton et al., 1985). Increases in pressure will lead to both an increase in the number of asperities and an increase in the real area of contact of the asperities (Saltiel et al., 2017; Lisabeth and Ajo-Franklin, 2023), but will not lead to complete closure of the fracture until stresses on the asperities are high enough to allow for significant crushing and plasticity. It appears the behavior of our sample is related to the interplay of the larger open fractures with the smaller pervasive grain boundary microcracks.

The behavior of our sample can be explained by the closure of grain boundary microcracks due to differential thermal expansion of rock forming minerals occurring in parallel with both micro- and meso-scale fracture closure with confining pressure. The grain boundary cracks are highly conformal and are likely formed during thermal contraction and decompression during core removal and preparation, so heating and pressurizing the sample brings it closer to its native state. As boundaries are pushed together, bonds may be formed leading to stiffer behavior (Dimitriev, 1972). This inference is supported by the observation that the bulk modulus at the highest temperature and pressure is approaching the bulk modulus the most prevalent mineral, albite (Brown et al., 2016). This behavior has been observed in Delegate aplite (Lu and Jackson, 1999) and Strathbogie granite (Kumari et al., 2017). The larger fracture, however, is not as well correlated, so the thermal expansion cannot close it significantly. The asperities continue to grow and the fracture stiffen, but the pressure dependence remains across the whole range of measured confining pressures.

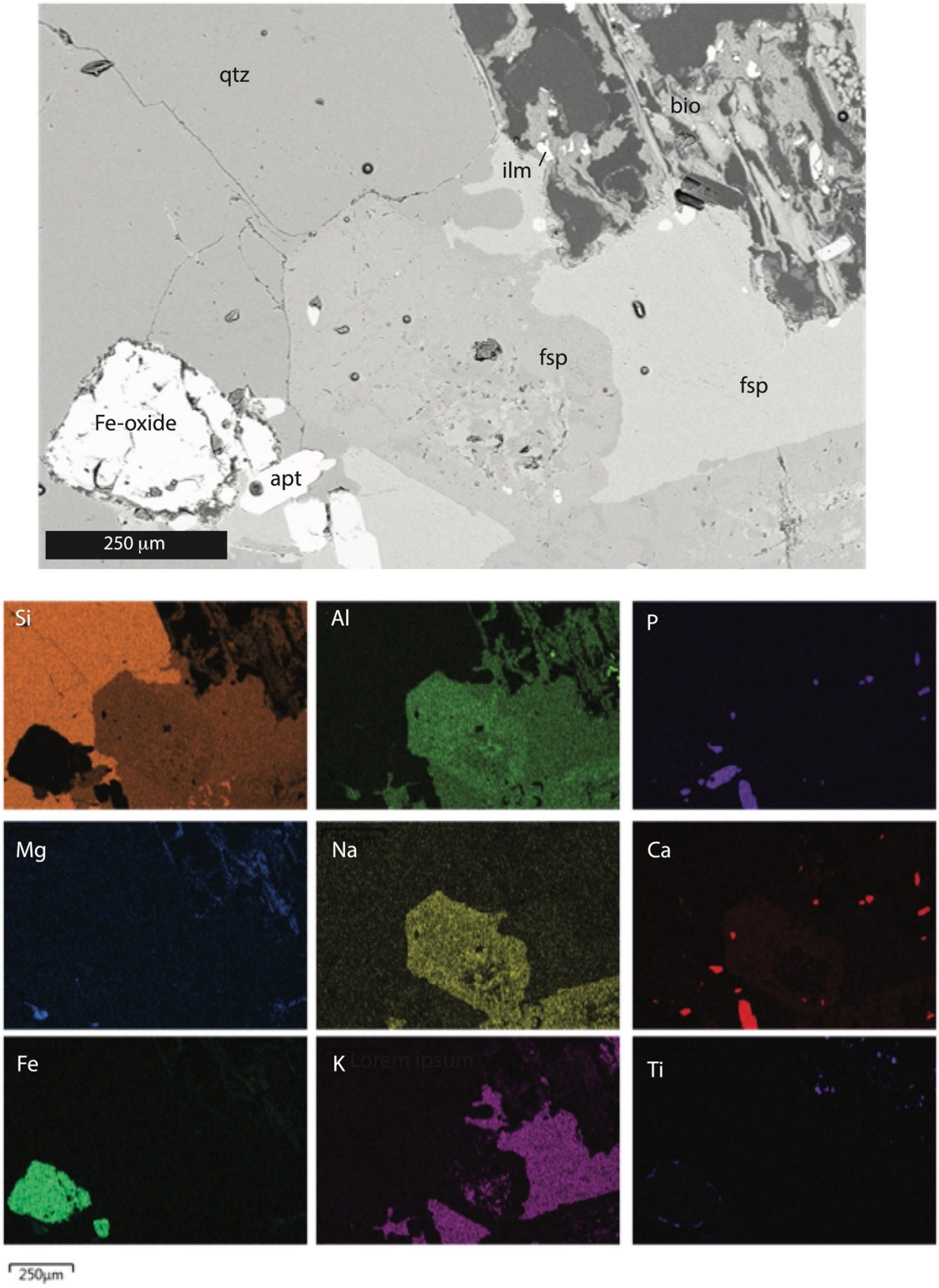

Figure 5: SEM and EDS maps of sample material.

4.3 Implications for geothermal systems

Geothermal systems in general and EGS in particular are highly dynamic systems. The injection of cool water into a warm reservoir necessarily perturbs the thermal, mechanical and chemical state of the reservoir. Thermal contraction has been shown to substantially increase reservoir permeability (Grant et al., 2013). The near field thermal evolution continues for timescales of years (Taron and Elsworth 2009). This may also result in a reduction in the elastic moduli of the rock adjacent to the fluid pathways, which will perturb the stress state of the near field. This could be relevant to consider as subsurface engineering gets more complex or interacts with existing fracture networks. The opening of thermal cracks increases porosity, which can lead to a reduction in pore pressure and concomitant increase in effective stress. The progressive closure of crack will have the opposite effect. As circulation continues for years and decades, the thermal state of a larger volume of rock may evolve. The coupling of this thermal evolution and the elastic properties of the reservoir materials must be fully understood to accurately forecast the geomechanical state of the system. Going forward, stress management will be essential to mitigate seismicity associated with EGS (Gaucher et al., 2015).

5. CONCLUSIONS

We conducted a series of rock mechanics experiments to fully characterize the bulk and shear modulus of a granodiorite sample from the Patua geothermal field. The sample was tested between 10 and 70 MPa and 23 and 150°C. The bulk modulus ranged from 19.2 to 84.1 GPa and the shear modulus ranged from 12.5 to 24.2 GPa. Temperature and pressure were positively correlated with both moduli. This behavior appears to be the result of thermal closure of grain boundary microcracks and progressive stress-driven closure of larger fractures. This mechanism may have repercussions for THMC coupling along fractures in reservoirs.

ACKNOWLEDGEMENTS

We thank Ahmad Ghassemi for providing the core material and Trenton Cladouhos for information about the core. This work is supported by the U.S. Department of Energy, Office of Energy Efficiency and Renewable Energy (EERE), Geothermal Technologies Office, under Award Number DE-AC02–05CH11231 with Lawrence Berkeley National Laboratory.

REFERENCES

Azim, M. R., Amin, M. S., & Shoeb, M. A. (2010, July). Prospect of enhanced geothermal system in baseload power generation. In 2010 IEEE International Conference on Advanced Management Science (ICAMS 2010) (Vol. 3, pp. 176-180). IEEE.

Barton, N., Bandis, S., & Bakhtar, K. (1985). Strength, deformation and conductivity coupling of rock joints. In International journal of rock mechanics and mining sciences & geomechanics abstracts (Vol. 22, No. 3, pp. 121-140). Pergamon.

Blake, O. O., & Faulkner, D. R. (2016). The effect of fracture density and stress state on the static and dynamic bulk moduli of Westerly granite. Journal of Geophysical Research: Solid Earth, 121(4), 2382-2399.

Brace, W., Walsh, J. B., & Frangos, W. T. (1968). Permeability of granite under high pressure. Journal of Geophysical research, 73(6), 2225-2236.

Brown, J. M., Angel, R. J., & Ross, N. L. (2016). Elasticity of plagioclase feldspars. Journal of Geophysical Research: Solid Earth, 121(2), 663-675.

Cladouhos, T. T., Uddenberg, M. W., Swyer, M. W., Nordin, Y., & Garrison, G. H. (2017). Patua geothermal geologic conceptual model. GRC Transactions, 41, 1057-1075.

Clark, S. P. (1966). Handbook of physical constants. Geological society of America.

David, E. C., & Zimmerman, R. W. (2011). Compressibility and shear compliance of spheroidal pores: Exact derivation via the Eshelby tensor, and asymptotic expressions in limiting cases. International Journal of Solids and Structures, 48(5), 680-686.

Dmitriyev, A. P. (1972). Physical properties of rocks at high temperatures (Vol. 684). National Aeronautics and Space Administration.

Espinoza, W. F., Pereira, J. M., Kneafsey, T., & Dai, S. (2023). Mechanical and creep properties of granitic minerals of albite, biotite, and quartz at elevated temperature. Geomechanics for Energy and the Environment, 34, 100465.

Fredrich, J. T., & Wong, T. F. (1986). Micromechanics of thermally induced cracking in three crustal rocks. Journal of Geophysical Research: Solid Earth, 91(B12), 12743-12764.

Gaucher, E., Schoenball, M., Heidbach, O., Zang, A., Fokker, P. A., van Wees, J. D., & Kohl, T. (2015). Induced seismicity in geothermal reservoirs: A review of forecasting approaches. Renewable and Sustainable Energy Reviews, 52, 1473-1490.

Ghassemi, A. (2012). A review of some rock mechanics issues in geothermal reservoir development. Geotechnical and Geological Engineering, 30, 647-664.

Grant, M. A., Clearwater, J., Quinão, J., Bixley, P. F., & Le Brun, M. (2013, February). Thermal stimulation of geothermal wells: a review of field data. In Proceedings 38th Workshop on Geothermal Reservoir Engineering, Stanford University, Stanford, California, February

Hopkins, D. L., Cook, N. G., & Myer, L. R. (1987, June). Fracture stiffness and aperture as a function of applied stress and contact geometry. In ARMA US Rock Mechanics/Geomechanics Symposium (pp. ARMA-87). ARMA.

Kc, B., Foroutan, M., Kamali-Asl, A., Ghazanfari, E., & Cladouhos, T. T. (2019, June). Geomechanical characterization of a granodiorite rock specimen from Patua geothermal field. In ARMA US Rock Mechanics/Geomechanics Symposium (pp. ARMA-2019). ARMA.

Kumari, W. G. P., Ranjith, P. G., Perera, M. S. A., Shao, S., Chen, B. K., Lashin, A., ... & Rathnaweera, T. D. (2017). Mechanical behaviour of Australian Strathbogie granite under in-situ stress and temperature conditions: An application to geothermal energy extraction. Geothermics, 65, 44-59.

Lisabeth, H., & Ajo-Franklin, J. The role of stress and fluid saturation on the acoustic response of fractured rock. Frontiers in Earth Science, 11, 1058984.

Lu, C., & Jackson, I. (1999). Seismic-frequency laboratory measurements of shear mode viscoelasticity in crustal rocks II: thermally stressed quartzite and granite. Q of the Earth: Global, Regional, and Laboratory Studies, 441-473.

Majer, E. L., Baria, R., Stark, M., Oates, S., Bommer, J., Smith, B., & Asanuma, H. (2007). Induced seismicity associated with enhanced geothermal systems. Geothermics, 36(3), 185-222.

Martin III, R. J., & Haupt, R. W. (1994, June). Static and dynamic elastic moduli in granite: The effect of strain amplitude. In ARMA North America Rock Mechanics Symposium (pp. ARMA-1994). ARMA.

Morrow, C. A., & Lockner, D. A. (2006). Physical properties of two core samples from well 34-9RD2 at the Coso Geothermal Field, California (pp. 1-32). US Geological Survey.

Ohno, I. (1995). Temperature variation of elastic properties of α-quartz up to the α-β transition. Journal of Physics of the Earth, 43(2), 157-169.

Saltiel, S., Selvadurai, P. A., Bonner, B. P., Glaser, S. D., & Ajo-Franklin, J. B. (2017). Experimental development of low-frequency shear modulus and attenuation measurements in mated rock fractures: Shear mechanics due to asperity contact area changes with normal stress. Geophysics, 82(2), M19-M36.

Smith, T., Sonnenthal, E., Nakata, N., Cladouhos, T., & Swyer, M. A (2023) Thermal, Hydrological and Mechanical Model of Patua Geothermal Field, Nevada. Proceedings, 48th Workshop on Geothermal Reservoir Engineering, Stanford University, Stanford, California, February 6-8

Taron, J., & Elsworth, D. (2009). Thermal–hydrologic–mechanical–chemical processes in the evolution of engineered geothermal reservoirs. International Journal of Rock Mechanics and Mining Sciences, 46(5), 855-864.

Tester, J. W., Anderson, B. J., Batchelor, A. S., Blackwell, D. D., DiPippo, R., Drake, E. M., ... & Toksoz, M. N. (2006). The future of geothermal energy. Massachusetts Institute of Technology, 358, 1-3.

Trník, A., Štubňa, I., Ondruška, J., Šín, P., & Csáki, Š. (2019). Young's Modulus of Prefired Qquartz Porcelain in a Tempertature Range of 20-1200° C. Materials & Technologies/Materiali in Tehnologije, 53(4).

Walsh, J. B. (1965). The effect of cracks on the compressibility of rock. Journal of geophysical research, 70(2), 381-389.

Wang, H. F., Bonner, B. P., Carlson, S. R., Kowallis, B. J., & Heard, H. C. (1989). Thermal stress cracking in granite. Journal of Geophysical Research: Solid Earth, 94(B2), 1745-1758.

White, M., Fu, P., McClure, M., Danko, G., Elsworth, D., Sonnenthal, E., ... & Podgorney, R. (2018). A suite of benchmark and challenge problems for enhanced geothermal systems. Geomechanics and Geophysics for Geo-Energy and Geo-Resources, 4, 79-117.

Yang, S. Q., Ranjith, P. G., Jing, H. W., Tian, W. L., & Ju, Y. (2017). An experimental investigation on thermal damage and failure mechanical behavior of granite after exposure to different high temperature treatments. Geothermics, 65, 180-197.